Localized state distribution and its effect on recombination in organic solar cells

R. A. Street*
Palo Alto Research Center, Palo Alto, California 94306, USA
(Received 11 May 2011; published 12 August 2011)

Transient photocurrent (TPC) and transient photovoltage (TPV) measurements are reported in bulk heterojunction organic solar cells. TPC is used to measure the band tail and deep trap density of states within the interface band gap and to identify the carrier species from the relative contribution of drift and diffusion. Steep exponential band tails are observed near the donor valence band edge, changing to a broader distribution of states at larger trap energies. The effect of the localized state distribution on the recombination is analyzed—particularly for geminate recombination, where it is shown that band tails can substantially enhance the probability that geminate pairs ionize to form free carriers. The TPV response is shown to have completely different characteristics from those of TPC, and the explanation is provided.

DOI: 10.1103/PhysRevB.84.075208 PACS number(s): 71.20.Rv, 73.50.Gr, 73.50.Pz

I. INTRODUCTION

Organic bulk heterojunction (BHJ) solar cells comprise phase-separated domains of an electron donor and acceptor.[1] In many examples of BHJ cells, and for the devices studied here, the donor is a polymer and the acceptor is a fullerene. Transport of electrons and holes are in the different domains, and recombination takes place primarily at the domain interface. A description of the transport and recombination in the BHJ cell must take into account the electronic structure of the materials, best expressed as the density of states (DOS) distribution. The relevant DOS is derived from the properties of both materials in the cell: the valence band, or highest occupied molecular orbital (HOMO), transport levels are from the polymer donor and the conduction band, or lowest unoccupied molecular orbital (LUMO), levels are from the fullerene acceptor.

The DOS is also important because it is the link between the structure and the electronic properties of the BHJ cell. The fabrication of the cell, the material composition of the device, the phase separation of the components, the effects of annealing, etc., all influence the physical structure and hence the electronic structure. Complete knowledge of the device involves understanding how the DOS reflects the atomic and nanoscale structure of the device, how the DOS influences electronic transport, and what recombination mechanisms are active. The DOS separates the problem into two parts: how transport and recombination follow from the DOS and how the DOS results from the physical structure. It is important and often possible to obtain the DOS empirically from electronic and optical measurements. One of the aims of this paper is to present experimental data from transient photocurrent (TPC) measurements that add to the information about the DOS. Of particular interest is the distribution of localized trap states forming the band tail and deeper states.

Several studies have obtained information about the DOS in BHJ solar cells and in the pristine materials. For example, Campbell *et al*. use space charge limited currents to deduce a band tail of localized states in poly(phenylene vinylene).[2] Similar measurements in poly(3-hexylthiophene) (P3HT) and transport models including band tails have been reported.[3,4] Campbell *et al*. developed a model of a Gaussian band of HOMO and LUMO states in which transport occurs at the center of the band and the edge of the band transitioned to a exponential tail of localized states. Nelson describes a similar DOS in which transport is limited by multiple trapping in the band tails and excitation to transport energy.[5] Localized band tail states in polymer thin film transistors account for the temperature and voltage dependence of the characteristics,[6] and exponential band tails are observed in other organic materials.[7] The measurements of dispersive transport and the spectral response of photoconductivity in two different BHJ solar cells by my colleagues and I also show the presence of an exponential band tail.[8] Although the evidence for exponential band tails is strong, most of the measurements are fitted to a band tail model and do not directly give the DOS distribution

This paper describes measurements of the band tail DOS distribution and investigates the relation between the DOS and the recombination processes. Section II describes transient photoconductivity and photovoltage measurements, which are analyzed in Sec. III to develop the DOS. Sec. IV discusses how the presence of band tail states influences geminate recombination and other transport and recombination mechanisms.

II. TRANSIENT PHOTOCONDUCTIVITY AND PHOTOVOLTAGE

TPC measurements have been applied to many low-mobility photoconductive materials to measure charge transport and mobility.[9,10] Here I apply the technique to the measurement of the band tail DOS distribution, building on evidence that the transport is dispersive because of multiple trapping in band tail states.[8] Transient photovoltage (TPV) is also used to study transport and recombination,[11,12] and the similarity of the technique suggests that the same physical processes are measured. I show that, despite the similarity, the two experiments exhibit different response times and operate by different mechanisms.

A. Method to obtain the DOS distribution from TPC

Previous experiments show that the carrier mobility in BHJ cells is dispersive and arises from multiple trapping in a band tail of localized states, with a good fit to an exponential band tail distribution.[13,14] The BHJ cell is made from disordered semiconductors, and such materials typically exhibit localized band tail states.[15] The carrier transport in a typical disordered semiconductor reflects the DOS distribution $N(E)$ and the carrier mobility $\mu(E)$. Two models are commonly used

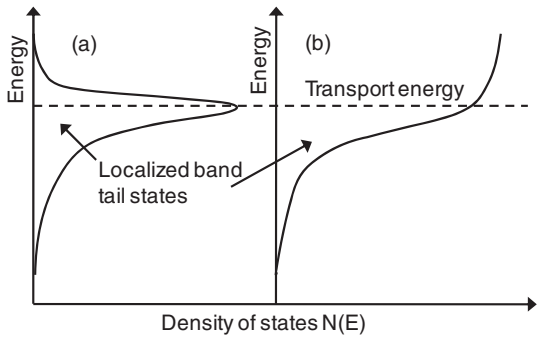

FIG. 1. Schematic density of states distribution N(E) for a disordered semiconductor showing mobile and localized states separated by a transport energy. (a) Narrow polaron band typically used to describe organic materials; (b) Band model typically applied to inorganic materials.

to describe transport in a disordered semiconductor: polymers are often described by polaron hopping transport in a narrow band,[16] whereas inorganic materials are described by a wider band of mobile states, with a mobility edge at which transport occurs. Both of these are illustrated in Fig. 1. From the point of view of the effects of band tails, these two descriptions are essentially equivalent.

In practice, the transport energy of the polaron band or the mobility edge is not precisely defined. Nevertheless, the mobility often changes sufficiently rapidly with energy so that the model of single transport energy is an adequate description, except possibly at low temperatures. In either case, carriers in localized band tail states need to be thermally excited to the transport energy, and the effective trap energy is the energy of the trap state with respect to the transport energy and possibly an additional hopping energy component. The following model assumes a transport energy, without being specific as to whether there is bandlike or hopping transport. First principles calculations of the band structure find a relatively wide band in polycrystalline polymers such as P3HT, which suggests the bandlike model.[8]

The dispersive TPC is described by a power-law time dependence, $J_{PC} \approx t^{\beta}$, with the exponent β equals $(\alpha - 1)$ before the transit time and $(-\alpha - 1)$ after the transit, averaged over the distribution of carriers in the sample. Here α is known as the dispersion parameter.[17] Dispersive transport occurs when there is a wide distribution of release times for the carrier as it moves across the sample. The physical mechanism of dispersive transport in a band tail is that carriers are repeatedly trapped and released by thermal excitation to the transport energy.[18] The rate of release from a trap of binding energy E at temperature T is $\omega_0 \exp(-E/kT)$, where ω_0 is an attempt to escape prefactor on the order of 10^{12} s^{-1} and k is Boltzmann's constant. At a measurement time t, trapped carriers with binding energy less than the demarcation energy $E_D(t)$ have a high probability of being released and those with larger energy have a low probability of release, where $E_D(t)$ is given by

$$t = \omega_0^{-1} \exp(E_D(t)/kT); \quad \text{hence,} \quad E_D(t) = kT \ln(\omega_0 t). \quad (1)$$

At time t, carriers are predominately excited from the states near $E_D(t)$, because the shallower states were released at shorter times, and are mostly empty, and the deeper states have both a lower concentration and a much lower excitation probability. Hence, $E_D(t)$ is the average trap energy with respect to the transport energy.

At times much longer than the carrier transit time, the photocurrent is equal to the rate of release of carriers from band tail states, because the additional time taken for the excited carrier to cross the sample is small and there is minimal retrapping in deep states, provided that the internal field is reasonably large. The photocurrent is therefore equal to the DOS at the demarcation energy times the rate at which the demarcation energy changes with time, or

$$J_{PC}(t) = evf N(E_D)\frac{dE_D}{dt}, \quad (2)$$

where e is the electronic charge, v is the device volume, and f is the fraction of states filled, which is assumed to be independent of energy. Using the relation between energy and time from Eq. (1) gives

$$N(E) = \frac{tJ_{PC}(t)}{evfkT}. \quad (3)$$

The DOS at trap energy E is therefore obtained from the photocurrent at time t, and the relation between E and t is given by Eq. (1). The model of Eqs. (2) and (3) is a good approximation, provided that the DOS changes more slowly with energy than the Fermi function,[19] which is also the condition for dispersive transport in a band tail.

For the specific case of an exponential band tail with a DOS, $N(E) = N_0 \exp(-E/E_0)$, Eq. (3) becomes

$$I_{PC}(t) = evfkTN_0\omega_0^{\alpha} t^{-\alpha-1}; \quad \alpha = kT/E_0. \quad (4)$$

The power-law form of Eq. (4) is the well-known expression for dispersive transport in an exponential band tail after the transit time, and the model of Eqs. (1)–(4) is essentially how the band tail model of dispersive transport was originally derived by Tiedje and Rose.[18] Previous work shows that Eq. (4) provides a good description of transport in the organic BHJ cells that are studied here.[8]

Equation (3) describes the relation between the photocurrent and the DOS for the general case of an arbitrary band tail distribution, with the energy scale given by Eq. (1), and is the model used to analyze the data. The time dependence of the TPC provides a quantitative measurement of the DOS—subject to the uncertainty in f, which affects the magnitude of $N(E)$, and in ω_0, which affects the energy scale. The model only applies when the band tail slope is wider than kT, which is the case for the materials studied. Monroe and Kastner discuss the analysis for more complex DOS distributions, which include discrete levels.[20]

B. Transient photoconductivity measurements

The transient photoconductivity measurements on BHJ solar cells were made as described in more detail in Ref. 8 but are extended to longer times. The same two solar cells are studied—PCDTBT:PCBM and P3HT:PCBM—and their full names are given in Ref. 21. The device fabrication is described in detail elsewhere.[22,23] The current is measured on a digital oscilloscope from the voltage across a small load resistor R and is valid for times longer than RC, where C is the sample

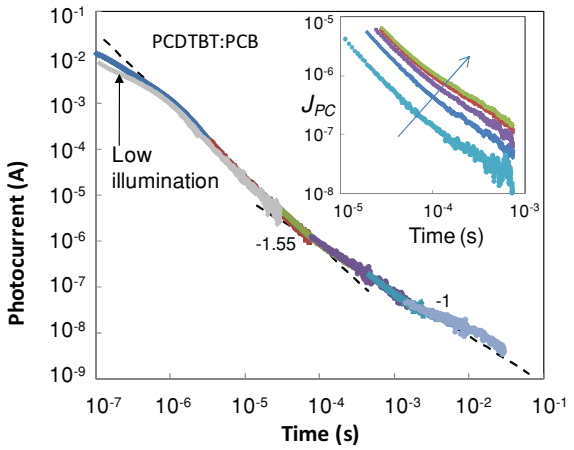

FIG. 2. (Color online) Transient photocurrent in PCDTBT:PCBM measured at times extending well beyond the transit time, and comprising a set of measurements indicated by the different colors. The transit time is the change of slope near 1 μs. Dashed lines are fits two different power law decays with exponent values indicated. (Inset) Detail of the transient near 0.1 ms, showing the result of increasing illumination intensity.

capacitance. The extended time range is obtained by increasing the load resistor, which had values from 4 Ω to 9 kΩ. Because the measured voltage equals $I_{PC}(t)R$, an increase in R increases the voltage and hence the measurement sensitivity, and the longer RC response time still allows measurement at the longer times. Figure 2 shows transient photoconductivity data for a PCDTBT:PCBM solar cell measured at short circuit. The current transients measured for the different load resistances overlap well and together give a measured current over 7 decades in magnitude and 5 decades in time, from 0.1 μs to 10 ms.

Previous work showed that the transient photoconductivity measures the response of both carriers in the BHJ cell, of which one has higher mobility than the other.[8] The data in Fig. 2 is for the slower carrier, and the transit time is indicated by the change of slope of $J(t)$ that occurs ∼1 μs. In the vicinity of the transit time, the data agree with earlier measurements, with a dispersion parameter of $\alpha \approx 0.55$. The photocurrent continues to decay as the same power law at longer times up to ∼0.1 ms. At longer times, there is a reduction in the slope, which continues to the limit of the measurement that occurs at ∼30 ms. The inset to Fig. 2 shows in more detail and for different illumination intensities the region of the change of slope that occurs at ∼0.1 ms, and Fig. 3 shows the intensity dependence of the photocurrent at 100 μs. The current increases linearly at low illumination levels and then saturates. I interpret the saturation as evidence for trap filling and therefore expect that the photocurrent data will give a reasonably accurate measure of the DOS. However, further studies of the trap filling are needed, because the illumination itself can cause excitation from traps, leading to saturation of the current but with incomplete filling. The relatively high light intensity can cause space charge effects, which may distort the transient response. The space charge effects only occur at short times, because most of the charge has left the sample at the longer times; therefore, the effect is not present. Figure 2 includes short time TPC data measured at lower illumination

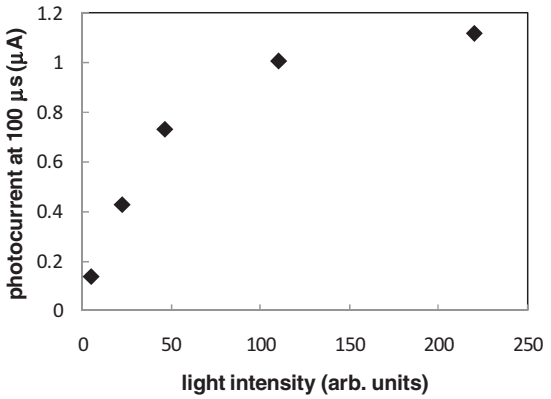

FIG. 3. Illumination intensity dependence of the transient photocurrent at 0.1 ms in the same PCDTBT:PCBM device as in Fig. 2, showing saturation of the photocurrent at high illumination intensity.

intensity and scaled vertically to match the higher-intensity data at longer times, where the space charge effects are absent. The comparison shows that there is indeed a small space charge effect that persists up to ∼10 μs. I therefore combine the long time data at the higher intensity with the scaled lower light intensity–shorter time data to extract the DOS.

Similar TPC data for P3HT:PCBM are shown in Fig. 4, which uses a low light intensity for the shorter time data and a higher intensity for longer times, as discussed earlier. The transit time is observed at ∼0.3 μs, after which there is a power-law decrease in photocurrent with a slope of −1.7, which agrees with the previous measurements that were used to obtain the mobility. At a time of ∼10 μs, there is a distinct change of slope that continues to the end of the measurement time.

C. Transient response in the diffusion regime

To analyze the DOS further, it is necessary to know whether the electron or hole transport is measured in the long time transient photoconductivity experiments. As discussed

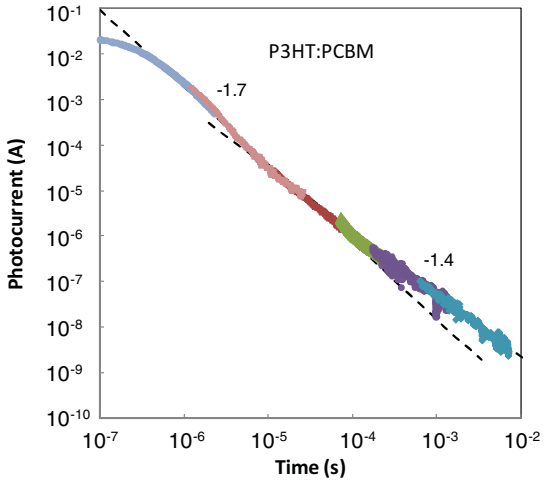

FIG. 4. (Color online) Transient photocurrent in P3HT:PCBM measured at times extending well beyond the transit time, and comprising a set of measurements indicated by different colors. The transit time is the change of slope near 0.3 μs. Dashed lines are fits two different power law decays with exponent values indicated.

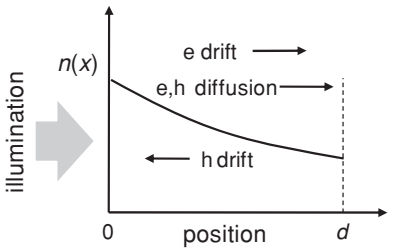

FIG. 5. Illustration of the initial carrier profile of optically excited electrons and holes within the solar cell, for illumination from the left side. Drift currents for electrons and holes are in opposite directions, while the diffusion currents are in the same direction.

in previous studies,[8] the response of the two carriers can be distinguished because one has lower mobility than the other, but the identity of the carrier is not immediately evident from the measurements because both electrons and holes contribute to the current with the same sign. Other measurements suggest that the fullerene has higher mobility than the polymer in P3HT:PCBM,[24] but less is known about PCDTBT:PCBM. The carrier identity can be inferred from measurement when a bias close to the built-in potential is applied and the internal field is close to zero. The method is illustrated in Fig. 5. There is a density profile of carriers in the BHJ cell when carriers are excited by illumination above the band gap. At the excitation energy of the TPC experiment, the optical absorption coefficient is $\sim 10^5$ cm^{-1}; therefore, the characteristic absorption length is the same order as the sample thickness. The initial carrier concentration profile is the same for electrons and holes, because both are generated by the splitting of the excitons at the internal interfaces.

The carrier transport current J at position x contains contributions from both drift and diffusion according to

$$J(F,x) = e\,[n(x)\mu F + Ddn(x)/dx]\,, \qquad (5)$$

where $n(x)$ is the carrier concentration, μ is the mobility, D is the diffusion coefficient, and F is the electric field. The diffusion term arises from the concentration gradient of the carriers, with the highest concentration at the illuminated junction, which is the hole injecting contact. The drift of electrons and holes contribute with the same sign to the current, because carriers of opposite sign move in opposite directions. However, diffusive motion of both carriers is in the same direction; therefore, the diffusion of electrons and holes contribute to the current with opposite sign. Diffusion dominates over drift when the internal voltage is less than or similar to kT/e, so the effects of diffusion should be observed within about ± 0.05 V from the built-in potential. Measurements of the TPC at bias voltages near the built-in potential therefore explore the difference contributions of drift and diffusion based on the change of sign of the current.

Data in Fig. 6 show the transient PC response for PCDTBT:PCBM and P3HT:PCBM at bias voltages that are close to the built-in potential for each cell. The background current is subtracted from the measurements. At the lower bias voltages the transient has the polarity of the reverse current, and at higher voltages it changes sign, as expected. In the intermediate region there are components of both polarities, indicating the diffusion-dominated regime. Previous

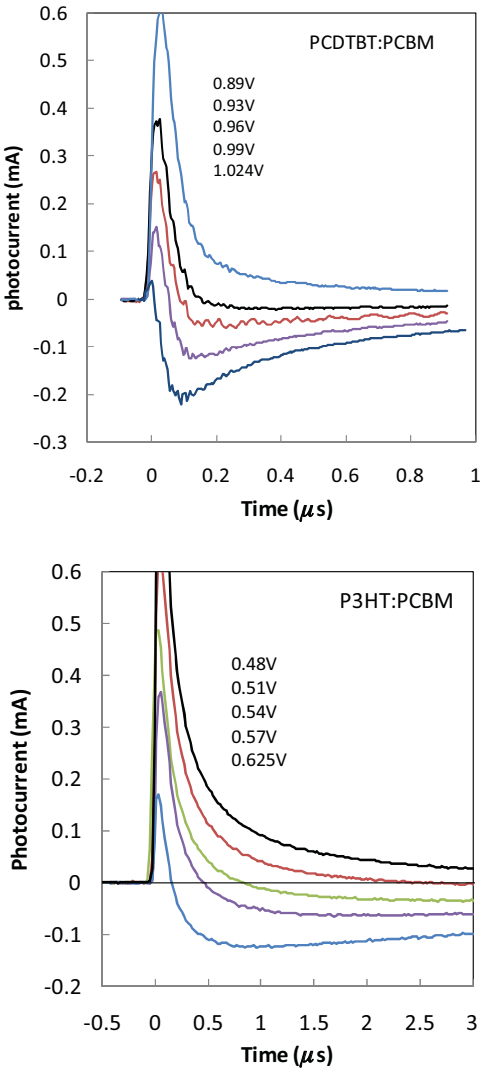

FIG. 6. (Color online) Transient photoconductivity of (a) PCDTBT:PCBM and (b) P3HT:PCBM at the bias voltages indicated, showing the change of sign of photocurrent that occurs for the slower carrier at a lower bias than for the faster carrier.

data also reported the change in the sign of the photocurrent for measurements near the built-in potential.[25]

The data in Fig. 6 provide identification of the fast and slow carriers. According to the discussion of Eq. (5), the photoresponse of the two carriers is expected to have the opposite sign when diffusion dominates and the same sign when drift dominates. Figure 6 shows that there is a change of sign, with the initial current having one polarity and the longer time current having the opposite polarity. Because illumination is through the indium tin oxide contact, the diffusive response of holes will have the opposite sign compared to hole drift at bias voltage below the built-in potential V_{BI}, whereas electrons will have the same sign for both diffusion and drift. The opposite is the case above V_{BI}. The observation that the slower response changes sign first therefore indicates that the slower response results from holes rather than electrons. The measurements therefore confirm that holes are the lower-mobility carrier in both cells.

Because the absorption depth in the 100-nm cell is on the same order of magnitude as the thickness, the concentration gradient $dn(x)/dx$ is roughly n_{AV}/d, where d is the sample thickness and n_{AV} is the average carrier concentration. The ratio of the contribution of drift and diffusion to the current at an internal cell voltage V is therefore $\sim eV/kT$, obtained by setting $D = \mu kT/e$ in Eq. (5). The diffusion transients are therefore expected to be 20–50 times smaller than the transient at zero bias, and the results in Fig. 5 are consistent with this estimate.

D. TPV measurement

TPV measurements use the same pulse illumination as those of TPC, but the experiment is done with a large load resistor such that the RC time constant is larger than the measurement time. White bias illumination with a range of intensities sets the value of V_{OC}, and the transient response to a weak illumination pulse was measured with a 1-MΩ load resistance. The measurement is therefore of the voltage transient at the open circuit voltage rather than the photocurrent. The aim of the measurements is to compare the photocurrent and photovoltage response. It might be expected that TPV and TPC are alternative measurements of the same transport and recombination processes. However, I show that this is not the case, and their different origin is discussed in Sec. III B.

Figure 7 shows the TPV measurements as a function of open circuit voltage. The range of V_{OC} is limited, because it changes slowly with white light intensity. The TPV response is approximately a simple exponential decay, which is strikingly different from the power-law form of the TPC. The time constant decreases from ~1 ms to 18 μs for V_{OC} increasing from 0.269 to 0.516 V. Again, this is a completely different result from the form of the photocurrent transients, which have a different magnitude of response time, depend much less on the voltage, and the voltage dependence is in the opposite direction. The TPC response extends to longer times at increasing applied bias, because the internal field decreases. The TPV response in the dark is also shown in Fig. 7, and the decay time is limited by the RC time constant, from which the cell capacitance can be found from the known load resistance. The data at $V_{OC} = 0.269$ V are close to the dark decay, but I have not attempted to correct the data. Measurements of PCDTBT:PCBM cells were comparable, and the data are analyzed and discussed in Sec. III B.

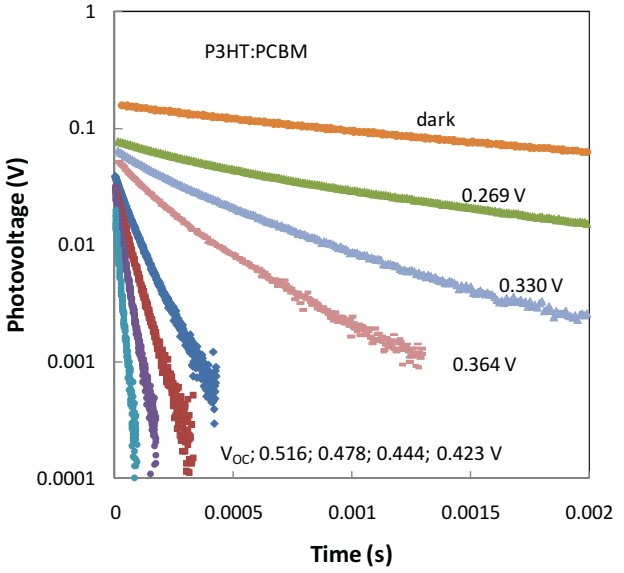

FIG. 7. (Color online) Measurement of the transient photovoltage response at different values of the open circuit voltage as indicated, determined by changing the intensity of the white bias illumination. The transient response in the dark is also shown. The measurements use a load resistance of 1 MΩ.

III. ANALYSIS OF THE TPC AND PHOTOVOLTAGE

This section analyzes the TPC data further to obtain the DOS distribution and describes a model for the TPV experiments.

A. The DOS distribution

Having established that the slower carriers are holes, it follows that the long time photoconductivity in Figs. 2 and 4 represents hole transport, at least for the data that are an extension of the transit time region. Hence, the DOS that I deduce is for the polymer HOMO levels. To apply Eq. (3) to measure the DOS, only the current at longer times than the transit time can be used for the analysis. Figure 8 shows the product of the photocurrent and the measurement time, scaled according to Eq. (3) and plotted against the demarcation energy to give the DOS distribution. The sample volume is known, and complete trap filling ($f = 1$) is assumed based on the intensity dependence data of Fig. 3. An exponential decrease in $N(E)$ is observed with a slope of $E_0 \approx 45$ meV, in agreement with the earlier measurements of the dispersion parameter. The energy scale of the DOS depends on the value of ω_0 in Eq. (1). I adopt a value of 10^{11} s^{-1} so that the DOS extrapolated to the band edge (at $E = 0$) agrees reasonably well with the band structure calculated previously for P3HT,[8] relying on the expectation that PCDTBT will have a similar band edge DOS.

The DOS flattens and even increases slightly at trap energies from 0.4 to 0.55 eV. The structure near 0.42 and 0.53 eV might reflect discrete levels, but more detailed studies are needed for

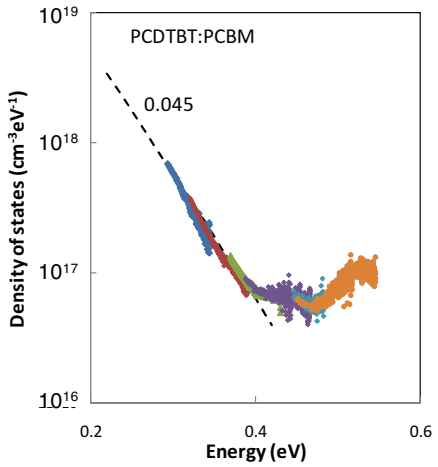

FIG. 8. (Color online) Experimental measurement of the density of states distribution for a PCDTBT:PCBM solar cell derived from the data of Fig. 2 using the analysis described in the text. The dashed line is an exponential with the indicated slope parameter E_0.

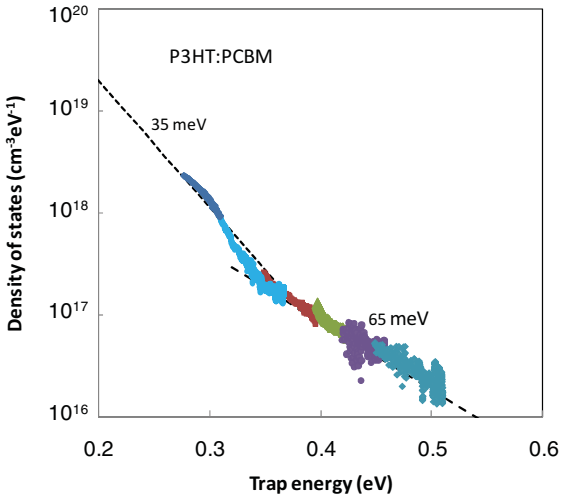

FIG. 9. (Color online) Experimental measurement of the density of states distribution for a P3HT:PCBM solar cell derived from the data of Fig. 4 using the analysis described in the text. The dashed lines are exponentials with the indicated slope parameters E_0.

confirmation. In the flat DOS region, the DOS is $\sim 10^{17}$ cm^{-3} eV^{-1}. This is a lower limit and would be larger if the occupancy f were significantly less than unity.

Figure 8 shows that the long time transient photoconductivity only explores a relatively small portion of the DOS. The normal time-of-flight measurement extends the timescale back to ~ 0.1 μs and the energy scale to ~ 0.23 eV, but I have to rely on extrapolation for the region of shallower trap energy. The increasing DOS at energy >0.5 eV may be electron traps related to the PCBM LUMO rather than the polymer HOMO. At this point, I have no further information and include this DOS with the HOMO band tail for simplicity. The interface band gap for PCDTBT:PCBM is ~ 1.4 eV so that the technique can measure states down to almost the middle of the interface gap.

Figure 9 shows the comparable DOS data for the P3HT:PCBM cell, using the same 10^{11} s^{-1} value for ω_0. In this case, the DOS follows an exponential decrease with a slope of 35 meV, again in agreement with the dispersive transport measurement, and then transitions at a trap energy of 0.35 eV to a larger slope of 65 meV, which continues to 0.5 eV where the DOS is $\sim 10^{16}$ cm^{-3} eV^{-1}. The change of slope to a larger E_0 is consistent with the previous analysis of the cell spectral response.[8] P3HT is generally thought to be polycrystalline, with regions of amorphous material that perhaps contain PCBM molecules.[26] I speculate that the steeper initial slope reflects the π–π stacking disorder of the crystallites, as recently calculated,[8] and the broader slope reflects the amorphous material at the grain boundaries. Small variations in the DOS are observed from different samples of the same blends, which presumably reflect different degrees of disorder or perhaps impurities. These measurements of the DOS should provide a tool for the study of the effects of sample preparation conditions, environmental exposure, etc.

The DOS obtained from these measurements is approximate and based on certain assumptions. The demarcation energy describes states within an energy band given by kT and therefore averages the actual DOS. Hence, the deep states might include discrete levels that are averaged in energy. The measurement also assumes that states are uniformly and fully populated, which is the case only if the capture cross section is constant and/or the states are completely filled. I have no specific information about the magnitude of the capture cross section, which relates to the prefactor ω_0 in Eqs. (1)–(3), or its energy dependence. Some effects, such as carrier retrapping, might also distort the DOS but should have a small effect. The energy scale depends on the assumed value of ω_0, which is taken to be 10^{11} s^{-1}. An order of magnitude change in ω_0 corresponds to a shift of 0.06 eV in the energy scale. Further work is needed to obtain more accurate values of ω_0 and hence increase the accuracy of the energy scale. The TPC measurement analysis subtracts the dark signal just before the illumination. Any long-term light-induced charge injection might distort the transient and affect the DOS estimate. I think this is unlikely to persist for as long as 1 ms when the photocurrent is so small ($\sim 10^{-9}$ A). Although these issues need to be resolved, the general form and magnitude of the DOS should be correct.

B. Model for TPV

Comparison of the TPC and photovoltage measurements in Figs. 2, 4, and 7 show very different characteristics regarding the response time and its voltage dependence. Elsewhere, I proposed that the TPV response is unrelated to the TPC response and is not a measure of the recombination of the solar cell under normal operating conditions.[27] My reasoning and a model for the TPV are now described in more detail and compared to the measurements. The solar cell current density $J(V)$ is the difference between the photocurrent and the dark current, which sum to zero at V_{OC} [22]:

$$J(V_{OC}) = 0 = J_{PC}(V_{OC}) - J_D(V_{OC}). \tag{6}$$

The additional light pulse in the TPV experiment increases J_{PC} by ΔJ_{PC} and hence charge flows within the solar cell for a short time. The additional charge transported q creates an additional voltage $\Delta V = q/C$, which is the measured photovoltage, where C is the device capacitance with

$$q = \int \Delta J_{PC}\, dt. \tag{7}$$

The time to create this voltage is roughly the transit time of the carriers in the internal field and is on the order of microseconds. The measurement is arranged with a sufficiently large external load resistance so that the charge that builds up cannot be dissipated quickly by the external circuit. Instead, the extra cell voltage causes an increase ΔJ_D in the forward diode current. The forward current therefore exceeds the DC photocurrent, and a net current flows in the forward direction until the photovoltage is reduced to zero. The additional current is

$$J(V_{OC} + \Delta V) = J(V_{OC}) + \Delta V \left.\frac{dJ}{dV}\right|_{V_{OC}} = \Delta V \left.\frac{dJ}{dV}\right|_{V_{OC}}. \tag{8}$$

The transient voltage response obtained from Eqs. (6) and (8), along with the experimental result that $J_{PC}(V)$ varies with

voltage much more slowly than J_D, is therefore

$$\frac{d\Delta V}{dt} = \frac{1}{C}\frac{dq}{dt} = \frac{J(V_{OC}+\Delta V)}{C} = \frac{\Delta V}{C}\left.\frac{dJ}{dV}\right|_{V_{OC}} = -\frac{\Delta V}{C}\frac{dJ_D}{dV}. \quad (9)$$

dJ_D/dV can be computed from the measured dark current, but a simple expression is obtained from the conventional dark diode current $J_D(V)$, given by

$$J_D(V) = J_0[\exp(eV/n_I kT) - 1], \quad (10)$$

where n_I is the diode ideality factor and Eq. (10) applies for V small enough that the series resistance is not limiting. From Eqs. (9) and (10), when $J_D > J_0$,

$$\frac{d\Delta V}{dt} = -\frac{eJ_D(V)\Delta V}{n_I kT\,C}. \quad (11)$$

Hence, the photovoltage is given by

$$\Delta V = \Delta V_0 \exp(-t/\tau_R); \quad \tau_R = n_I kT\,C/eJ_D(V). \quad (12)$$

This equation shows that the TPV response is expected to have an exponential decay, as observed in Fig. 7, with a time constant that is inversely proportional to the dark current at the open circuit voltage of the TPV measurement.

The model can be tested using the data of Fig. 7 for a P3HT cell and similar data for a PCDTBT cell. The data points in Fig. 10 are the inverse of the TPV response time for the two types of cell, plotted as the quantity $n_I kTC/e\tau_R$. The ideality factor n_I is 1.5–1.7 for P3HT:PCBM and PCDTBT:PCBM,[28] based on the measured dark current; C is obtained from the dark photovoltage transient in Fig. 7, for which the measured 2.4 ms decay time is RC; R is 1 MΩ; and the measurements are made at room temperature. According to the model of Eq. (12), $n_I kTC/e\tau_R$ is equal to the dark current $J_D(V)$. Fig. 10 plots the measured dark current of the two cells for comparison. The agreement is excellent, and there are no arbitrary fitting parameters, indicating that the model is correct—the combined experimental uncertainty in $n_I TC$ is ∼20%. There is some difference between $n_I kTC/e\tau_R$ and $J_D(V)$ at the high and low ends of the voltage range because of the series and the shunt resistance of the cell, which is not included in Eq. (10). To make a correct comparison between the data and the model, the whole active area of the device must be illuminated in the TPV measurement; otherwise, $J_D(V)$ must be scaled to the illumination area.

The TPV response does reflect a recombination process, because the dark current occurs by electrons and holes recombining at the BHJ interface. However, the recombination that is measured by TPV is not the process that determines the photocurrent in the solar cells. Under normal solar cell operation, charge that reaches the contacts is collected and contributes to the external current; therefore, it is not part of the recombination current. However, in the TPV experiment, this charge cannot be part of the external current and instead adds to the forward current and recombines at the interface. Transient absorption measurements made under the same experimental conditions observe the same charge carriers with the same response time,[11] which just reflects that the charge returns through the device to the interface.

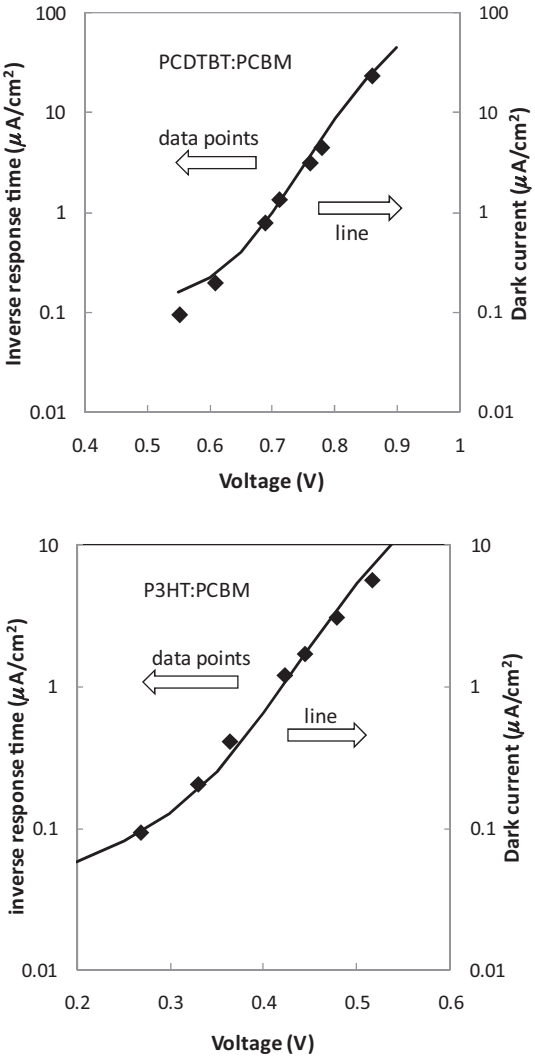

FIG. 10. Plot of the inverse of the photovoltage response time constant scaled according to Eq. (12) (data points) for (upper) a PCDTBT:PCBM solar cell and (lower) a P3HT:PCBM solar cell, compared to the measured dark current (lines) for the same devices.

IV. DISCUSSION

Having established the presence of band tails in the BHJ solar cells, it is important to determine their effect on recombination processes, in addition to carrier transport. Their influence on the geminate recombination mechanism is discussed first, followed by their possible role in other recombination mechanisms.

A. Band tail role in geminate recombination

This section analyses the process of geminate recombination, particularly how the band tail states modify the competition between ionization and recombination. BHJ solar cells have reasonable efficiency because the excitons are split at the interface to form a free electron in the fullerene acceptor and a hole in the polymer or small molecule donor. In high-efficiency cells, the efficiency of charge separation is >90% under short circuit conditions. There continues to be a question as to why the separation of carriers is so efficient

in the better solar cells, because the Coulomb interaction is expected to bind the electron and hole even after they split, so geminate recombination should reduce the solar cell current and efficiency. The bound electron–hole pair separated by the interface is referred to as the charge transfer exciton (CTE), and the nature of this excited state has been much discussed.[29]

One proposed explanation for the efficient ionization of the CTE is that the kinetic energy released when the exciton is split at the domain interface causes the electron and hole to separate far enough apart to reduce the Coulomb binding energy.[30] The kinetic energy is roughly equal to the band offset between the LUMO levels for excitons created in the polymer. On the basis of this model, it is suggested that the band offset between the polymer and the fullerene LUMO should not be smaller than ∼0.5 eV; otherwise, there would be insufficient kinetic energy to separate the pair. However, recent experiments that look for such a hot-carrier effect have proved to be negative, and the same quantum efficiency is found when the electron–hole pair is excited across the interface and with lower-energy photons.[31] The hot-carrier effect is therefore not a limitation on the magnitude of the band offset.

Another widely discussed model is that the CTEs are split by the electric field of the cell by the Braun-Onsager mechanism and that the field dependence of the recombination probability explains the solar cell photocurrent voltage dependence.[32] However, it has been shown that the field dependence of geminate recombination can be tested experimentally using a TPC measurement.[33] There is no detectable field-dependent geminate recombination in at least the two common solar cells studies here, implying that it is not larger than ∼10% even at low internal fields. As discussed later, other studies have also found no evidence for geminate recombination. The CTE luminescence is sometimes observed, but in each case it is weak. It therefore appears that an equilibrium CTE ionizes at room temperature with high probability, even without an applied field.

A general explanation for a high probability of charge separation of the CTE state is that the binding energy of the separated pair is sufficiently small enough for the thermal ionization to dominate.[34] The rate of thermal ionization is

$$K_I = \omega_0 \exp(-E_B/kT), \tag{13}$$

where E_B is the binding energy of the CTE with respect to a well-separated polaron pair, with the hole in the polymer and the electron in the fullerene. The probability of ionization of the CTE for a recombination rate K_R is

$$P_I = \frac{K_I}{K_I + K_R} = \left(1 + K_R \omega_0^{-1} \exp(E_B/kT)\right)^{-1}. \tag{14}$$

For the case of a high ionization rate $K_I \gg K_R$, typical of high-efficiency solar cells, the probability of geminate recombination is approximately

$$P_{\text{Gem}} = 1 - P_I \approx K_R \omega_0^{-1} \exp(E_B/kT). \tag{15}$$

For assumed values of $P_{\text{Gen}} = 0.1$, $\omega_0 = 10^{12}$ s^{-1} and $K_R = 10^9$ s^{-1}, Eq. (15) shows that, E_B can be no larger than 7 kT, which is 0.175 eV at room temperature. This energy is smaller than the exciton binding energy in the bulk polymer, but, as pointed out previously,[34] the electron and hole are separated by the interface; therefore, the energy is expected to be smaller. From the Coulomb energy alone, this binding energy corresponds to a separation of the electron and hole by ∼2.5 nm. Different assumed parameters can increase the critical energy slightly and perhaps reduce the separation to 1.5–2 nm, but this is still larger than is expected for the size of the CTE at the interface.

The next section discusses two mechanisms that can enhance the ionization probability and that, to the best of my knowledge, have not been previously considered. One mechanism relates to the presence of the disorder-induced band tail in the DOS, and the second relates to the magnitude of the band offset.

B. Energy-lowering effect of band tails states

The binding energy of the CTE is referenced to the energy of a well-separated polaron pair. In the absence of band tail states, the energy difference is the Coulomb binding energy, together with a possible increase in the electron–phonon coupling energy. However, when there is a DOS distribution including localized band tail states for either or both the electron and the hole, then the carriers can lower their energy by occupying band tail states.

It may seem that the energy lowering should apply equally to both the CTE state and the polaron pair to give no net effect. However, the CTE comprises an electron and hole that are very close together and constrained to be at the interface, which limits the available states that comprise the CTE. The polaron pair does not have this limitation and therefore can access more of the DOS, including band tail states with larger binding energy. Hence, the dissociation of the CTE may be accompanied by a reduction of energy, because the electron and hole can occupy shallow localized states, and the lower energy offsets the Coulomb binding energy of the CTE. Figure 11 illustrates the bound CTE state and the reduced Coulomb binding energy as the pair separates into mobile polarons at the transport energy. Also illustrated is the reduction in the pair energy when they can access localized band tail states. The energy gain increases with separation because an increasing number of states are accessed; hence,

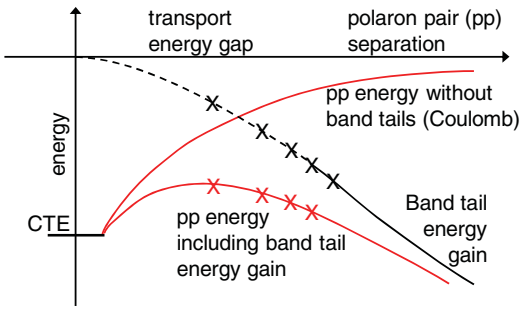

FIG. 11. (Color online) Schematic illustration of the energy lowering of the CTE when the carriers transfer to band tail localized states. The Coulomb energy, the band tail energy and the combined total energy are shown as function of carrier separation, relative to the energy of distant mobile polarons at the transport energy. The crosses in the band tail energy curve and the total energy reflect that there are a finite number of close band tail states and represent the first, second, third etc nearest neighbor, eventually reaching a continuum.

more states of lower energy are available. The total energy as a function of separation combines the Coulomb and band tail components. The CTE energy with respect to the separated polaron pair is reduced by the band tails, and a sufficiently distant polaron pair may actually have lower energy than the CTE.

To estimate the magnitude of the effect, consider the availability of band tail states near the CTE site for a DOS distribution $N(E)$, which could be either the hole DOS in the polymer or the electron DOS in the fullerene. To find a state in one or the other domain within the distance R_X from the CTE at the interface, this state must lie in a hemisphere of volume $V_X = 2\pi {R_X}^3/3$. The probability of finding the nearest state at distance R is derived from the nearest-neighbor distribution function $G(R)$, which for a half-sphere is[35]

$$G(R) = 2\pi R^2 N \exp(-2\pi R^3 N/3), \tag{16}$$

where N is the total density of available states. The probability of finding a state within a specific distance R_X is therefore

$$p(R_X) = \int_0^{R_X} G(R) dR = 1 - \exp\left(-2\pi R_X^3 N/3\right), \tag{17}$$

which is 50% when $R_X = 0.7N^{-1/3}$. This calculation gives the typical distance to the nearest available state.

The hole DOS distribution $N(E)$ is described in Figs. 8 or 9 and characterized by an exponential band tail $N_0\exp(-E/E_0)$, with $N_0 \approx 3\times10^{21}$ cm^{-3} eV^{-1} and $E_0 \approx 0.045$ eV for PCDTBT:PCBM and a smaller slope parameter for P3HT:PCBM. Hence, the total number of localized states up to the top of the band tail is $N_0E_0 = 1$–2×10^{20} cm^{-3}, from which it follows that there is a 50% probability of finding the nearest band tail state within a distance of $R_X \approx 1.5$ nm. The wavefunction extent of the CTE is probably in the range 0.5–1 nm, so it is unlikely that the CTE can lower its energy by occupying a band tail state. Instead, the typical CTE comprises only extended states from the transport energy region of the DOS.

The individual electron or hole, on the other hand, can lower its energy by tunneling to a nearby localized band tail state of lower energy than the transport energy. The localization in band tail states therefore reduces the energy of the separated polaron pair compared to the CTE, and the more band tails states that are accessible, the greater the energy reduction. The energy gained if the CTE splits into a localized electron and hole and the probability that this occurs, is estimated as follows. The probability of tunneling into a localized state at a distance R_T is $\omega_0\exp(-2R_T/R_L)$, where R_L is the localization radius of the CTE wavefunction. Using an argument similar to that for the competition between recombination and pair separation in Sec. IV A (Eq. (14)), tunneling can occur over a distance

$$R_T = 0.5\ R_L\ \ln(\omega_0/K_R) \approx 4\ R_L, \tag{18}$$

which is consistent with a tunneling distance of 2 nm or more when R_L is 0.5–1 nm. The typical energy gained by tunneling into the nearest band tail state is the median energy of the band tail, which is $E_0\ln2 \approx 30$ meV. The energy gain is roughly twice this amount if the electron and the hole both tunnel to their nearest neighbor. However, if more than one band tail state is accessible to the carrier, the energy gained is larger. When N_T states can be accessed, the median energy of the lowest energy state is

$$E_0 \ln\left[\frac{1}{1-2^{-1/N_T}}\right] \approx E_0 \ln(2N_T). \tag{19}$$

For example, if the tunneling distance doubles from the nearest-neighbor distance of 1.5 to 3 nm, then $\sim2^3 = 8$ band tail states are available and the median lowest energy state has a binding energy of $\sim0.045 \times \ln(16) \approx 0.12$ eV. The band tail energy lowering indicated in Fig. 11 describes the increasing binding energy of the lowest state as a function of distance and shows that only a discrete number of close states transition to a continuum of states at larger distances.

The Coulomb energy at 1.5-nm separation is $\sim$0.25 eV, and the additional trap energy gives a binding energy of the nearest-neighbor polaron pair as $0.25 + 2 \times 0.03 = 0.31$ eV. At 3-nm separation, the corresponding energy is 0.35 eV. Supposing the CTE energy is 0.3 eV, then the presence of the band tail states effectively reduces the ionization energy to zero for the nearest-neighbor site and, at further separation, the band tail polaron pair is the low energy state. Although these are only rough estimates, the calculation shows that there can be a substantial reduction in the CTE ionization energy in the presence of band tail states. The separate pair can easily be the lowest energy state, and ionization will occur with high probability.

This calculation is approximate, because it ignores the actual molecular structure and the DOS is not yet accurately known. The real situation is also more complicated: the CTE is probably mobile and diffuses along the interface before ionization or recombination occurs, and this mobility increases the number of band tail states that are accessible. More detailed calculations and a Monte Carlo simulation of the separation are probably needed to quantify the effect.

C. Relation between band offset and CTE recombination rate

Figure 12 illustrates the wavefunction of the CTE, which comprises an electron in the fullerene LUMO and a hole in the polymer HOMO, and a simple structureless material on either side of the interface is assumed. The wavefunctions of the two states are largely confined to the two sides of the interface; therefore, the matrix elements for recombination are reduced

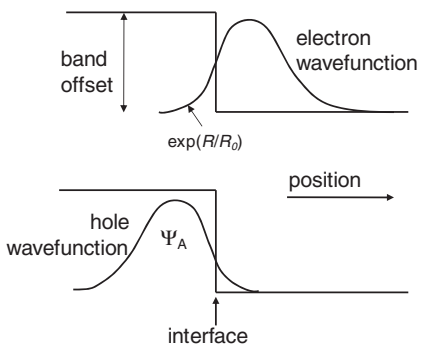

FIG. 12. Illustration of the electron and hole wavefunction comprising the CTE showing their exponential decay into the adjacent material due to the potential well created by the band offset.

compared to that of a bulk exciton. The matrix elements are dominated by the overlap of the wavefunction on one or the other side of the interface with the wavefunction that penetrates from the other side. As shown in Fig. 12, the model has the form of a particle in a potential well, in which the well depth for the electron is given by the LUMO band offset V_B, and the corresponding HOMO band offset is the potential well for the hole. When the band offset is large, the wavefunction penetration across the interface will be small. Consequently, the wavefunction overlap will be correspondingly small, and the radiative transition rate K_R will be low, favoring ionization of the CTE, according to Eq. (14) or (15). The magnitude of the effect is estimated as follows.

The well-known expression for the wavefunction extending into the potential wall (one-dimensional model) is

$$\Psi = \text{const. } \exp(-R/R_0); \quad R_0 = (2meV_B/\hbar^2)^{-1/2}, \quad (20)$$

which describes the electron wavefunction for the barrier energy V_B, where m is the electron mass and $\hbar$ is Planck's constant. From Eq. (20), R_0 is $\sim 0.2 {V_B}^{-1/2}$ nm/V$^{1/2}$, assuming an effective mass of 1. The matrix element of the radiative CTE transition is described by the overlap of the wavefunctions

$$M \approx \int \Psi_A \exp(-R/R_0) dR, \quad (21)$$

where Ψ_A represents the main portion of the wavefunction (i.e., the hole in the polymer HOMO or the electron in the fullerene LUMO) and the exponential term is the wavefunction component of the other carrier that extends thorough the barrier, as indicated in Fig. 12. The radiative recombination transition probability is proportional to M^2. There are two simple limiting cases, corresponding to a wavefunction Ψ_A that is uniform over a length R_M or one that is localized at a distance R_M from the interface. For these two cases, it follows from Eqs. (20) and (21) that

$$K_R = K_0(R_0/R_M)^2 = 0.04K_0/\left(V_B R_M^2\right) \quad (22)$$

and

$$K_R = K_0 \exp(-2R_M/R_0) = K_0 \exp\left(-10R_M V_B^{1/2}\right), \quad (23)$$

with R_M in units of nanometers and K_0 as the recombination rate when the wavefunctions overlap completely. In either case, the recombination lifetime of the CTE is reduced as the band offset increases. Taking $R_M = 1$ nm for an example, the rate factor K_R/K_0 is shown in Fig. 13 for the two cases as a function of the band offset voltage. Hence, the radiative recombination rate and the corresponding geminate recombination rate Eq. (14) are increasingly suppressed when there is a large band offset, and the suppression can be large. The actual rate presumably lies between the two extremes of the uniform and the localized wavefunctions, depending on the actual form of the wavefunction; therefore, the rate is expected to be reduced by 10–100 times except when the band offset is small. BHJ cells with a small band offset may therefore have enhanced geminate recombination compared to those with a larger band offset.

The combination of a reduced radiative recombination rate because of the low electron–hole wavefunction overlap and the availability of band tail states to assist the ionization

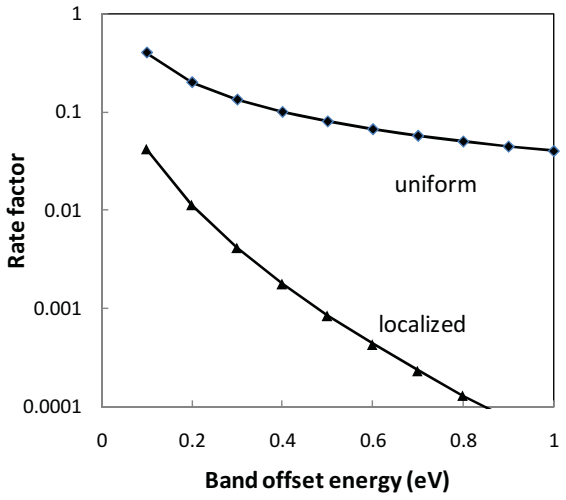

FIG. 13. Plot of the rate factor that reduces the radiative recombination rate of the CTE due to the reduced electron-hole wavefunction overlap. The two plots are for the uniform and discrete wavefunction approximations as discussed in the text.

is able to account for the observed low rate of geminate recombination. It would be interesting to have more detailed measurements of the geminate recombination rate as a function of band offset in a set of different BHJ cells to test the idea. This analysis of geminate recombination suggests that careful optimization of material properties is needed for BHJ cells. The solar cell efficiency is generally improved by minimizing the band offset, because this minimizes the reduction in the open circuit voltage. Also, the carrier mobility is increased and recombination through localized states is reduced by minimizing the band tail density of localized states. However, the preceding analysis suggests that too large a reduction in band offset and in the band tail DOS may have the negative effect of increasing the geminate recombination. A careful balance is needed for the optimum cell performance.

D. Other recombination mechanisms

This section revisits other recombination mechanisms and considers the possible role of band tails and other experimental results. Aside from geminate recombination, the other main recombination mechanisms that have been considered in BHJ solar cells are bimolecular or Langevin recombination, reverse diffusion to the contact, and transitions through localized states. There have been numerous modeling studies of the recombination mechanisms but little agreement. References 23,36–40 list 14 papers (illustrative but not a complete set) that study the recombination, mostly involving numerical solutions to the drift–diffusion equations for the cell response. Three of these papers conclude that geminate recombination alone is responsible[36]; three find only the Langevin mechanism,[37] three find that both geminate and Langevin contribute[38]; three find traps alone are responsible[23,39] and two attribute the recombination to a combination of geminate and reverse diffusion.[40] The models do not all apply to the same material, although many refer to P3HT:PCBM. This characterization of the results is approximate but sufficient to make the point that more definitive experimental evidence

for the recombination mechanism is needed to resolve the disagreements.

Regarding bimolecular recombination, the disagreement over whether the recombination kinetics in BHJ solar cells at low light intensity are first or second order is described elsewhere.[27,41] Evidence for high-order recombination comes from measurements of the recombination times, including TPV, coupled with measurements of charge density, both as a function of V_{OC} under illumination.[11] The combination of these data suggests that the carrier concentration varies with generation rate G as $G^{1/s}$, with s in the range 2–3, which seems to imply a high-order recombination process. Sec. III.B showed that TPV is not a reliable method to obtain the relevant recombination kinetics.

The release of carriers from the band tails can show kinetics that appear to have a high order. Consider the case that carriers are trapped in a band tail and the illumination is removed. Provided that there is an internal voltage, carriers are excited to the mobile states and collected at the contacts. Following the analysis in Sec. II A, at measurement time t the band tail is filled to the demarcation energy so that the number of trapped carriers is

$$N_T = \int_{E_D}^{\infty} N_0 \exp(-E/E_0) dE = E_0 N_0 \exp(-E_D/E_0). \quad (24)$$

The response time to the decay of the carrier concentration, τ_R, is the inverse of the rate of excitation from the traps, given by Eq. (1). Using the definition of the dispersion parameter in Eq. (3), the response time of the trapped charge is given by

$$\tau_R = \omega_0^{-1} (E_0 N_0)^{1/\alpha} N_T^{-1/\alpha}. \quad (25)$$

Because the dispersion parameter α is 0.5–0.7 for the cells that are studied, the response time will vary with charge concentration with an exponent of $-(1.5–2)$. Such dependence suggests second- or third-order kinetics. However, the response time is a measure not of the recombination kinetics but of the detrapping kinetics. The measurement of a response time is not necessarily a measure of the dominant recombination mechanism.

Previous publications proposed that the dominant recombination mechanism arises from transitions through localized states at or near the interface;[23,28] hence, the mechanism is similar to the Shockley-Read-Hall process familiar in crystalline semiconductors. We argued that the other recombination mechanisms were not consistent with the measurements, that a simple model for recombination through traps fitted the data well, and that the forward current also indicated a trap mechanism. The information presented here on the DOS distribution provides further support for the mechanism by demonstrating that there is a substantial density of localized states in the cells, distributed across much of the interface band gap. Furthermore, the traps densities observed here are consistent with the earlier defect density estimate of $3.10^{16}-3.10^{17}$ cm^{-3}.[23] Trap-dominated recombination should not be a surprise, because more carriers are trapped in localized states than are in the transport band under solar cell operating conditions. However, a direct correlation between the solar cell recombination and the specific DOS distribution remains to be observed, although it is known that trap recombination does occur when a large density of traps is introduced.[37]

A recent model for the dark forward current adds further evidence for the trap mechanism.[42] The model shows that direct recombination at the interface between mobile carriers leads to an ideality factor of 1, whereas recombination through traps, specifically a broad exponential band tail, increases the ideality factor. Hence, the measurements that find an ideality factor of 1.5 or larger indicate that the trap mechanism dominates, as my colleagues and I suggested earlier.[23] The model in Ref. 42 is for a planar heterojunction, but the general result probably also applies to the BHJ case.

V. CONCLUSIONS

Measurements of the TPC in BHJ solar cells, extending earlier results to longer times, allow measurements of the DOS distribution of localized band tail states. The TPC measurement also provides direct information about which band tail is measured by identifying the carrier with the lower mobility as holes and thus the DOS as the polymer HOMO levels. In both of the cell types, there is a transition to a characteristically different DOS at large trap energies. The ability to measure the localized state DOS opens the opportunity to study how the DOS differs in solar cells comprising different materials and to observe the effects of the preparation conditions and subsequent environmental exposure. Furthermore, the DOS distribution is a necessary input to numerical modeling of the solar cell current-voltage characteristics.

The experiments also show that TPV measurements on the same samples have a strikingly different response from TPC measurements. A model that explains the difference is provided and shown to account accurately for the data. TPV has been one basis for identifying bimolecular and higher-order recombination processes, and my results cast doubt on these interpretations.

The presence of band tail states affects the recombination mechanisms, as well as the carrier transport. Geminate recombination is discussed in detail, and it is shown that the presence of band tails reduces the effective binding energy of the charge transfer state and hence increases the probability of ionization.

The density of band tail states that is derived from the TPC measurement is approximate, because it relies on assumptions about the trap filling fraction and the thermal excitation prefactor—as well as an assumption of a reasonably well-defined mobility edge. The transport of carriers near the mobility edge is also uncertain, because it is not clear whether a band transport model that might be associated with the crystalline polymer grains, or a hopping model that has typically been associated with an amorphous polymer, is more appropriate. More experimental information about these assumptions is necessary to be able to refine the experimental measurement of the DOS.

ACKNOWLEDGMENTS

I am grateful to A. Heeger and S. Cowan for providing the solar cell samples and for useful discussion, to J. Northrup for useful discussion, and to C. Paulson for technical assistance.

*street@parc.com

[1] S. Gunes, H. Neugebauer, and N. S. Sariciftci, Chem. Rev. **107**, 1324 (2007).

[2] A. J. Campbell, D. D. C. Bradley, and D. G. Lidzey, J. Appl. Phys. **82**, 6326 (1997).

[3] Z. Chiguvare and V. Dyakonov, Phys. Rev. B **70**, 235207 (2004).

[4] M. C. J. M. Vissenberg and M. Matters, Phys. Rev. B **57**, 12964 (1998).

[5] J. Nelson, Phys. Rev. B **67**, 155209 (2003).

[6] H. Sirringhaus, Adv. Mater. **17**, 2411 (2005); A. Salleo, T. W. Chen, A. R. Volkel, Y. Wu, P. Liu, B. S. Ong, and R. A. Street, **70**, 115311 (2004).

[7] W. L. Kalb, S. Haas, C. Krellner, T. Mathis, and B. Batlogg, Phys. Rev. B **81**, 155315 (2010).

[8] R. A. Street, K. W. Song, J. E. Northrup, and S. Cowan, Phys. Rev. B **83**, 165207 (2011).

[9] F. W. Schmidlin, Phys. Rev. B **16**, 2362 (1977).

[10] B. Hartenstein, H. Bassler, A. Jakobs, and K. W. Kehr, Phys. Rev. B **54**, 8574 (1996).

[11] C. G. Shuttle, B. O. Regan, A. M. Ballantyne, J. Nelson, D. D. C. Bradley, J. de Mello, and J. R. Durrant, Appl. Phys. Lett. **92**, 093311 (2008).

[12] A. Foertig, A. Baumann, D. Rath, V. Dyakonov, and C. Deibel, Appl. Phys. Lett., **95**, 052104 (2009).

[13] N. Karl, K.-H. Kraft, J. Marktanner, M. Munch, F. Schatz, R. Stehle, and H.-M. Uhde, J. Vac. Sci. Technol. A **17**, 2318 (1999).

[14] C. R. McNeill and N. C. Greenham, Appl. Phys. Lett. **93**, 203310 (2008).

[15] N. F. Mott and E. A. Davis, *Electronic Processes in Non-crystalline Materials* (Oxford University Press, Oxford, 1979).

[16] See for example, H. Bassler, Phys. Stat. Sol. **175**, 15 (1993); G. Horowitz, Adv. Mater. **10**, 365 (1998).

[17] H. Scher and E. W. Montroll, Phys. Rev. B **12**, 2455 (1975).

[18] T. Tiedje and A. Rose, Solid State Commun. **37**, 49 (1980); see also J. Orenstein and M. A. Kastner, Phys. Rev. Lett. **46**, 1421 (1981).

[19] E. A. Schiff, M. A. Parker, and K. A. Conrad, *MRS Symposia Proceedings*, Vol. 118 (Materials Research Society, Pittsburg, PA, 1988), p. 477.

[20] D. Monroe and M. A. Kastner, Philos. Mag. **47**, 605 (1983).

[21] PCDTBT is poly(N-9′-hepta-decanyl-2,7-carbazole-alt-5,5-(4′,7′-di-2-thienyl-2′,1′,3′-benzothiadiazole); PC(70)BM is [6-6]-phenyl C61(70)-butyric acid methyl ester; and P3HT is poly(3-hexylthiophene). The PCDTBT cell is fabricated with PC70BM, and the P3HT cell is fabricated with PC60BM.

[22] S. H. Park, A. Roy, S. Beaupre, S. Cho, N. Coates, J. S. Moon, D. Moses, M. Leclerc, K. Lee, and A. J. Heeger, Nat. Photonics **3**, 297 (2009).

[23] R. A. Street, M. Schoendorf, A. Roy, and J. H. Lee, Phys. Rev. B **81**, 205307 (2010).

[24] M. Punke, S. Valouch, S. W. Kettlitz, N. Christ, C. Gartner, M. Gerken, and U. Lemmer, Appl. Phys. Lett. **91**, 071118 (2007)

[25] S. R. Cowan, R. A. Street, S. Cho, and A. J. Heeger, Phys. Rev. B **83**, 035205 (2011).

[26] B. Watts, W. J. Belcher, L. Thomsen, H. Ade, and P. C. Dastoor, Macromolecules **42**, 8392 (2009).

[27] R. A. Street, Phys. Rev. B **82**, 207302 (2010).

[28] R. A. Street and M. Schoendorf, *Proceedings of the 35th IEEE Photovoltaic Specialists Conference* (IEEE, Honolulu, HI, 2010).

[29] V. I. Arkhipov, P. Heremans, and H. Bassler, Appl. Phys. Lett. **82**, 4605 (2003); P. Peumans and S. R. Forrest, Chem. Phys. Lett. **398**, 27 (2004).

[30] T. M. Clarke, A. M. Ballantyne, J. Nelson, D. D. C. Bradley, and J. R. Durrant, Adv. Funct. Mater. **18**, 4029 (2008).

[31] J. Lee, K. Vandewal, S. R. Yost, M. E. Bahlke, L. Goris, M. A. Baldo, J. V. Manca, and T. Van Voorhis, J. Am. Chem. Soc. **132**, 11878 (2010).

[32] C. L. Braun, J. Chem. Phys. **80**, 4157 (1984).

[33] R. A. Street, S. Cowan, and A. J. Heeger, Phys. Rev. B **82**, 121301 (2010).

[34] R. A. Street, Appl. Phys. Lett. **93**, 133308 (2008).

[35] P. Hertz, Math. Ann. **67**, 387 (1909).

[36] V. D. Mihailetchi, L. J. A. Koster, J. C. Hummelen, and P. W. M. Blom, Phys. Rev. Lett. **93**, 216601 (2004); J. Szmytowski, Semicond. Sci. Technol. **25**, 015009 (2010); R. A. Marsh, C. R. McNeill, A. Abrusci, A. R. Campbell, and R. H. Friend, Nano Lett. **8**, 1393 (2008).

[37] H. H. P. Gommans, M. Kemerink, J. M. Kramer, and R. A. J. Janssen, Appl. Phys. Lett. **87**, 122104 (2005); L. J. A. Koster, V. D. Mihailetchi, and P. W. M. Blom, Appl. Phys. Lett. **88**, 052104 (2006); K. Maturova, S. S. van Bavel, M. M. Wienk, R. A. J. Janssen, and M. Kemerink, Nano Lett. **9**, 3032 (2009).

[38] M. M. Mandoc, L. J. A. Koster, and P. W. M. Blom, Appl. Phys. Lett. **90**, 133504 (2007); T. Kirchatz, B. E. Pieters, K. Taretto, and U. Rau, J. Appl. Phys. **104**, 094513 (2008); M. Hilczer and M. Tachiya, J. Phys. Chem. C **114**, 6808 (2010).

[39] M. M. Mandoc, F. B. Kooistra, J. C. Hummelen, B. de Boer, and P. W. M. Blom, Appl. Phys. Lett. **91**, 263505 (2007); L. Tsabari and N. Tessler, J. Appl. Phys. **109**, 064501 (2011).

[40] P. W. M. Blom, V. D. Mihailetchi, L. J. A. Koster, and D. E. Markov, Adv. Mater. **19**, 1551 (2007); M. Limpinsel, A. Wagenpfahl, M. Mingebach, C. Deibel, and V. Dyakonov, Phys. Rev. B **81**, 085203 (2010).

[41] C. Deibel and A. Wagenpfahl, Phys. Rev. B **82**, 207301 (2010).

[42] N. C. Giebink, G. P. Wiederrecht, M. R. Wasielewski, and S. R. Forrest, Phys. Rev. B **82**, 155305 (2010).